USCAP

ARTICLE

Development and validation of a vascularity-based architectural classification for clear cell renal cell carcinoma: correlation with conventional pathological prognostic factors, gene expression patterns, and clinical outcomes

Chisato Ohe[1]✉, Takashi Yoshida[2], Mahul B. Amin[3,4], Naho Atsumi[1], Junichi Ikeda[1,2], Kazuho Saiga[1], Yuri Noda[1], Yoshiki Yasukochi[5], Riuko Ohashi[6], Haruyuki Ohsugi[2], Koichiro Higasa[5], Hidefumi Kinoshita[2] and Koji Tsuta[1]

The prognostic significance of an architectural grading system for clear cell renal cell carcinoma (ccRCC) has recently been demonstrated. The present study aimed to establish a vascularity-based architectural classification using the cohort of 436 patients with localized ccRCC who underwent extirpative surgery and correlated the findings with conventional pathologic factors, gene expression, and prognosis. First, we assessed architectural patterns in the highest-grade area on hematoxylin and eosin-stained slides, then separately evaluated our surrogate score for vascularity. We grouped nine architectural patterns into three categories based on the vascular network score. "Vascularity-based architectural classification" was defined: category 1: characterized by enrichment of the vascular network, including compact/small nested, macrocyst/microcystic, and tubular/acinar patterns; category 2: characterized by a widely spaced-out vascular network, including alveolar/large nested, thick trabecular/insular, papillary/pseudopapillary patterns; category 3: characterized by scattered vascularity without a vascular network, including solid sheets, rhabdoid and sarcomatoid patterns. Adverse pathological prognostic factors such as TNM stage, WHO/ISUP grade, and necrosis were significantly associated with category 3, followed by category 2 (all $p < 0.001$). We successfully validated the classification using The Cancer Genome Atlas (TCGA) cohort (n = 162), and RNA-sequencing data available from TCGA showed that the angiogenesis gene signature was significantly enriched in category 1 compared to categories 2 and 3, whereas the immune gene signature was significantly enriched in category 3 compared to categories 1 and 2. In univariate analysis, vascularity-based architectural classification showed the best accuracy in pathological prognostic factors for predicting recurrence-free survival (c-index = 0.786). The predictive accuracy of our model which integrated WHO/ISUP grade, necrosis, TNM stage, and vascularity-based architectural classification was greater than conventional risk models (c-index = 0.871 vs. 0.755–0.843). Our findings suggest that the vascularity-based architectural classification is prognostically useful and may help stratify patients appropriately for management based on their likelihood of post-surgical recurrence.

Modern Pathology (2022) 35:816–824; https://doi.org/10.1038/s41379-021-00982-9

INTRODUCTION

Clear cell renal cell carcinoma (ccRCC) is the predominant histologic subtype of adult renal cancers, accounting for 75% of RCCs[1]. Approximately 30% of patients with localized RCC at the time of surgery will develop metastases[2]. In routine clinical practice, TNM stage, World Health Organization (WHO)/International Society of Urological Pathology (ISUP) nucleolar grade, tumor-specific necrosis, and sarcomatoid and rhabdoid morphology have been recognized as important prognostic parameters for predicting recurrence or metastasis[3,4].

Since morphological analysis is currently the gold standard for cancer diagnosis[5], additional prognostic factors in ccRCC are needed. Recently, an architectural grading system has been proposed with assessment of 19 architectural patterns for ccRCC, which could stratify prognostic predictions after surgery[6]. Subsequently, a comprehensive morphological analysis including nine architectural, twenty-four cytological and tumor microenvironmental features was evaluated and developed into an integrated taxonomy[7]. Although the prognostic prediction ability is better than that of previous grading systems[6,7], these evaluation criteria are complicated and less optimal to use in routine clinical settings because they include various histological features such as cytological or inflammatory features in addition to architectural patterns.

[1]Department of Pathology, Kansai Medical University, Hirakata, Osaka 573-1191, Japan. [2]Department of Urology and Andrology, Kansai Medical University, Hirakata, Osaka 573-1191, Japan. [3]Department of Pathology and Laboratory Medicine, University of Tennessee Health Sciences Center, 930 Madison Avenue, Memphis, TN 38163, USA. [4]Department of Urology, University of Southern California, 1441 Eastlake Avenue, Los Angeles, CA 90033, USA. [5]Genome Analysis, Institute of Biomedical Science, Kansai Medical University, 2-3-1 Shin-machi, Hirakata, Osaka 573-1191, Japan. [6]Histopathology Core Facility, Faculty of Medicine, Niigata University, Niigata 951-8510, Japan. ✉email: ohec@hirakata.kmu.ac.jp

Received: 17 September 2021 Revised: 18 November 2021 Accepted: 19 November 2021
Published online: 30 November 2021

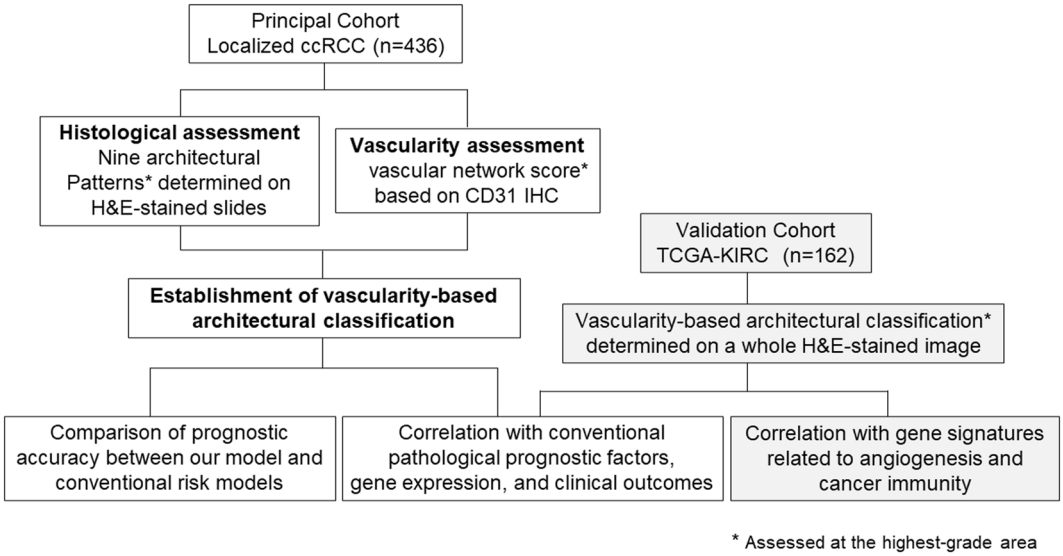

Fig. 1 Study designs. The present study aims to establish a vascularity-based architectural classification using the principal cohort and correlates the findings with conventional pathologic factors, gene expression, and prognosis. We validate the Cancer Genome Atlas (TCGA) cohort and evaluate the correlation between the classification and gene expression signatures using RNA-sequencing data.

ccRCC is characterized by rich neovascularization due to inactivation of the von Hippel Lindau (*VHL*) gene, resulting in constitutive activation of hypoxia-inducible transcription factor (HIF). Because vascular endothelial growth factor (VEGF) is activated by the VHL/HIF pathway, VEGF receptor-tyrosine kinase inhibitors (VEGFR-TKIs) have been used for metastatic ccRCC as standard systemic agents[1]. Recently, the association of architectural patterns reflecting tumor vascularity with response to VEGFR-TKIs in patients with metastatic ccRCC was reported[7], along with a correlation between tumor vascular architecture in ccRCC and gene expression and its underlying mechanism[8,9]. Because an integrated morphologic and molecular approach is expected to provide both prognostic and therapeutic implications[10], a simplified morphology-based architectural classification reflecting the underlying genomics and providing additional prognostic value is an unmet clinical need.

In the present study, we established an architectural classification focusing on the vascular network and correlated the results with conventional pathological prognostic factors, and clinical outcomes. Furthermore, we validated the classification using the Cancer Genome Atlas (TCGA) cohort and evaluated the correlation between a vascularity-based architectural classification and gene expression signatures related to angiogenesis and cancer immunity using RNA-sequencing data available from TCGA[11]. Finally, we compared the prognostic utility with a previously described grading system[6] and validated the prognostic accuracy between our model and conventional risk models. The study design is shown in Fig. 1.

MATERIALS AND METHODS

Case selection

With Institutional Review Board approval (No. 2018109 and No. 2020222), data for 453 patients who underwent extirpative surgery for non-metastatic ccRCC at Kansai Medical University Hospital between 2006 and 2017 were extracted from our institutional database of RCC for this study. Of these, 17 patients were excluded from this study for the following reasons: synchronous or metachronous bilateral tumors ($n = 13$), pre-surgical treatment with tyrosine kinase inhibitors ($n = 1$), or death due to operation-related complications ($n = 3$). Thus, 436 cases with localized ccRCC (cT1-4N0-1M0) were analyzed as the principal cohort. Cases of ccRCC available from the TCGA-KIRC cohort were also validated ($n = 162$, one-third of 488 ccRCC cases[12]). TCGA whole slide images were accessed via the Cancer Digital Slide Archive[13]. The detailed workflow of this study is shown in Supplementary Fig. 1.

Data collection

Clinical data, including age, gender, Eastern Cooperative Oncology Group (ECOG) performance status, node status, and distant metastasis were tabulated. Our institutional database of RCC contains pathological findings which were re-evaluated based on 2016 WHO classification[3] and the 2017 TNM staging system[14] as previously described[15–18]. All ccRCC were histologically diagnosed when the carcinoma contained typical ccRCC area of a small and thin-walled vascular network and/or showed diffuse membranous positivity of carbonic anhydrase IX (CA9) by immunohistochemistry[3]. Clear cell papillary RCCs were excluded by morphology and immunohistochemical findings of cup-like CA9 expression and diffuse cytokeratin 7 positivity[3]. Pathological prognostic factors, including pathological TNM stage, WHO/ISUP grade, and necrosis (microscopic tumor-specific necrosis)[4] were evaluated. For comparison with existing prognostic models, University of California Los Angeles Integrated Staging System (UISS)[19], Leibovich prognosis score[2], and Mayo Clinic Stage, Size, Grade, and Necrosis (SSIGN) score[20] were calculated.

Histological evaluation

Architectural patterns of the highest WHO/ISUP grade area were determined on hematoxylin and eosin (H&E)-stained slides of whole tissue sections without immunohistochemistry. Nine architectural patterns focusing on only tumor architecture regardless of nuclear, cytoplasmic, and inflammatory features were identified according to previously described patterns[6,7] (Fig. 2). Examples of histological assessment and how the architectural patterns were determined are shown in Supplementary Fig. 2. Cytoplasmic features such as clear (tumor cells with clear, pale cytoplasm), mixed (some tumor cells are clear, some are eosinophilic), or eosinophilic (tumor cells with granular eosinophilic) were also assessed at the highest-grade area according to our previous report[18]. For the assessment of the tumor microenvironment, tumor-associated immune cells including both mononuclear cells and granulocytes were evaluated in one representative slide of the highest-grade area. The immunophenotype was categorized based on the location of inflammatory cells on a representative H&E-stained slide as follows: desert, non-inflamed; excluded, peritumoral immune infiltration; and inflamed, intratumoral immune infiltration as previously described[21]. All H&E-stained images of both the principal and TCGA-KIRC cohorts were reviewed by a genitourinary pathologist (CO) blinded to clinical outcomes. For interobserver variability, forty cases randomly selected were reviewed using H&E-stained slides including the highest-grade area for assessment of vascularity-based architectural classification and WHO/ISUP grade among three pathologists (CO, KS, and YN).

Definition of vascular network score

For assessment of tumor vascularity, we defined a vascular network score immunohistochemically detected by CD31 (JC70A, prediluted, Leica Biosystem,

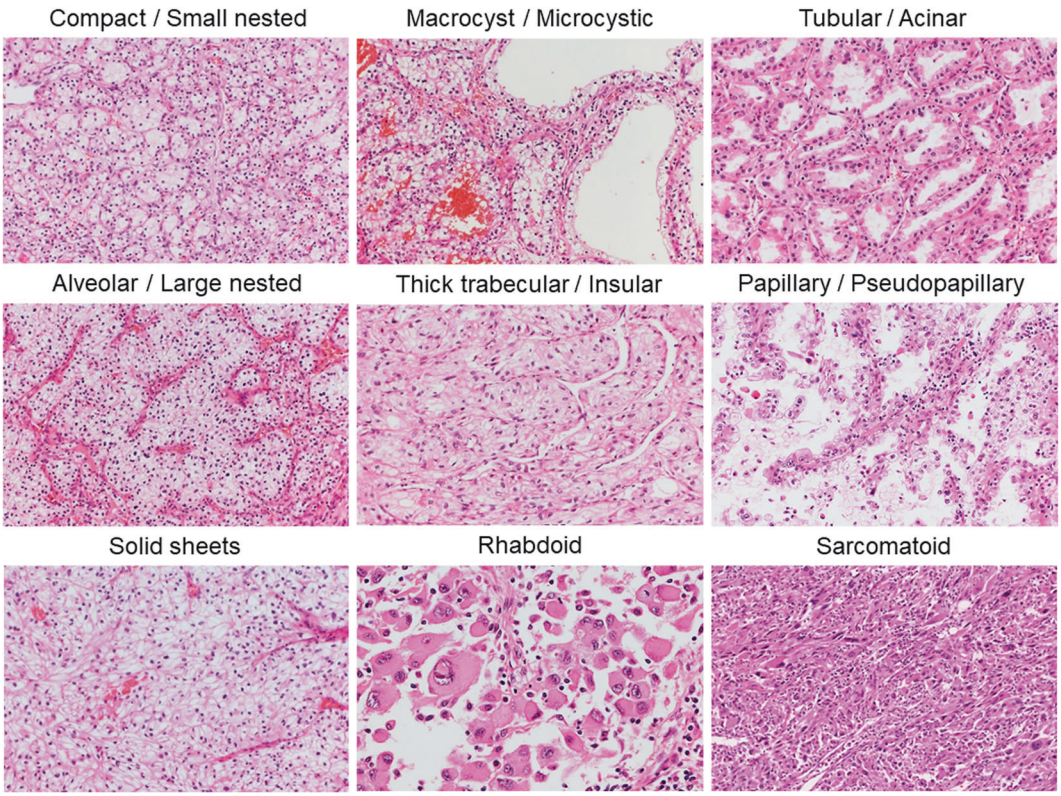

Fig. 2 Nine architectural patterns identified in this study. Architectural patterns assessed in this study. Nine architectural patterns were identified according to previous reports[6,7].

Newcastle Upon Tyne, UK), which was evaluated in the highest-grade area according to the description previously described[7]. We regarded the presence of vascular architectural complexity as a vascular network score 2, a widely spaced-out vascular network as score 1, and scattered vascularity without a vascular network as score 0. Representative images of vascular network scores are shown in Supplementary Fig. 3A. The correlation between vascular network score and microvessel area[18,22], the association of vascular network score with expression of angiogenesis-related genes[23,24] and the recurrence-free survival rate were confirmed (Supplementary Fig. 3B, C, and D, respectively).

Gene expression analysis

RNA-sequencing data of TCGA were downloaded as described previously[25]. Because VEGFR-TKIs and immune checkpoint inhibition are both established as standard care of metastatic RCC, the IMmotion 150 gene signatures consisting of angiogenesis, immune and antigen presentation, and myeloid inflammation were extracted as previously reported[26]. Gene expression signatures were defined according to the previous reports:[18,26,27] angiogenesis: *VEGFA, KDR, ESM1, PECAM1, FLT1, ANGPTL4*, and *CD34*; effector T-cell: *CD8A, INFG, GZMA, GZMB, PRF1*, and *EOMES*; immune checkpoint: *CD274 (PD-L1), CTLA4*, and *TIGIT*; and myeloid: *CXCL1, CXCL2, CXCL3, IL6, and PTGS2*. For calculating gene signature scores, each gene score was normalized by z-score across all patients and averaged to create signature scores for each patient[18,27].

Of 130 cases in the principal cohort, we also analyzed gene expression related to hypoxia (*EPAS1*, known as *HIF2α*[28]) and angiogenesis (*CDH5*[23], *RGS5*[24], and *PDGFD*[29]) for confirming the underlying mechanism of vascularity-based architectural classification using a custom NanoString panel of ClearCode34 genes[30] as described in our prior reports[17,18].

Statistical analysis

The study outcome measure was recurrence-free survival (RFS), defined as the time from surgery to initial local or distant metastasis shown on imaging. All continuous data are shown as median-valued and interquartile ranges (IQRs). Statistical analyses were performed using EZR version 1.54 (Saitama Medical Center, Jichi, Japan)[31]. A Chi-squared test for categorical variables, one-way ANOVA analysis with Tukey test for parametric variables, Mann–Whitney U test or Kruskal–Wallis test for non-parametric variables were used to evaluate the statistical significance among two or more groups. Pearson product–moment correlation coefficient was measured for a linear correlation between two sets of data. Interobserver agreement was statistically assessed using kappa statistics. Recurrence-free survival was assessed by the Kaplan–Meier method with the log-rank and the Cox proportional hazards models. Harrell's concordance index (c-index) was used to evaluate the predictive accuracy of Cox models. A two-sided $p < 0.05$ was considered statistically significant.

RESULTS

Clinicopathological characteristics

Clinicopathological features of 436 patients with localized ccRCC are presented in Table 1. The median age at ccRCC diagnosis was 65 years ((IQR, 56.0-73.0 years) 56.0–73.0 years). One hundred three (23.7%) of the tumors were of the high stage (TNM stage III or IV), and 142 (32.5%) of the high WHO/ISUP grade (3 or 4). Of the 436 patients, 57 (13.1%) experienced a recurrence and 15 (3.4%) died of ccRCC during a median follow-up period of 68.2 months (IQR, 38.6–103.6 months). The median time to recurrence after surgery was 61.7 months (IQR, 33.8–93.6 months). Regarding architectural patterns, 180 (41.3%) patients with compact/small nested pattern, 38 (8.7%) with macrocyst/microcystic pattern, 64 (14.7%) with tubular/acinar pattern, 48 (11.0%) with alveolar/large nested pattern, 58 (13.3%) with thick trabecular/insular pattern, 20 (4.6%) with papillary/pseudopapillary pattern, 10 (2.3%) with solid sheets, 5 (1.1%) with rhabdoid pattern, and 13 (3.0%) with sarcomatoid pattern were observed in the principal cohort. Clinicopathological characteristics of the TCGA-KIRC cohort are shown in Supplementary Table 1.

Association of architectural patterns and vascular network score

The association of nine architectural patterns with vascular network scores based on CD31 immunohistochemistry is shown in Fig. 3A. Compact/small nested, macrocyst/microcystic, and

Table 1. Clinicopathological characteristics of 436 cases with localized ccRCCs in the principal cohort.

Variables	
Age, years, median (IQR)	65 (56.0–73.0)
Gender, *n* (%)	
Female	117 (26.8)
Male	319 (73.2)
TNM stage, *n* (%)	
I	320 (73.4)
II	13 (3.0)
III	101 (23.2)
IV	2 (0.5)
WHO/ISUP grade, *n* (%)	
1	60 (13.8)
2	234 (53.7)
3	114 (26.1)
4	28 (6.4)
Sarcomatoid/rhabdoid features, *n* (%)	
Absent	416 (95.4)
Present	20 (4.6)
Necrosis, *n* (%)	
Absent	370 (84.9)
Present	66 (15.1)
Recurrence, *n* (%)	57 (13.1)
Cancer-specific mortality, *n* (%)	15 (3.4)
Overall mortality, *n* (%)	52 (11.9)

ccRCC clear cell renal cell carcinoma, *IQR* interquartile range, *WHO* World Health Organization, *ISUP* International Society of Urological Pathology.

tubular/acinar patterns are characterized by enrichment of the vascular network (vascular network score 2); alveolar/large nested, thick trabecular/insular, papillary/pseudopapillary patterns are characterized by a decreased vascular network (vascular network score 1); solid sheets, rhabdoid, and sarcomatoid patterns are characterized by scattered vascularity without a vascular network (vascular network score 0). Finally, nine architectural patterns reflecting the vascular network were grouped into three categories by using one-way analysis of variance with Tukey test ($p < 0.001$; Fig. 3B).

Establishment of vascularity-based architectural classification and interpretation of morphologic features reflecting vascularity

Based on the above-described results, we have established the vascularity-based architectural classification. The association of vascularity-based architectural classification with architectural patterns highlighted to vasculature by CD31 immunohistochemistry is presented in Fig. 3C. Architectural patterns of category 1 have delicate vascular stroma with vascular architectural complexity as previously described[9,32]. Architectural patterns of category 2 have widely spaced-out vascular networks. As hallmarks of category 2, we found that large tumor nests were surrounded by vascular areas composed of endothelial cells embedded in the eosinophilic extracellular matrix (Supplementary Fig. 4A) as previously described[9] or large vascular channels (Supplementary Fig. 4B). Architectural patterns of category 3 have scattered vascular arrangements without vascular networks. The distribution among architectural patterns, vascular network scores, and vascularity-based architectural categories are displayed in Supplementary Fig. 5. Because the correlation between architectural patterns of ccRCC and the vascular network score was confirmed, we could capture the architectural patterns on only H&E-stained slides. The interobserver variability was assessed using kappa statistics, which showed good agreement among the three pathologists ($k = 0.83–0.93$ for vascularity-based architectural classification and $k = 0.87–0.90$ for WHO/ISUP grade).

Association of vascularity-based architectural classification with pathological factors and gene expression patterns

Adverse pathological prognostic factors such as TNM stage, WHO/ISUP grade, and necrosis were significantly enriched in category 3, followed by category 2 (all $p < 0.001$; Fig. 4A). Representative images of cytoplasmic features are shown in Fig. 4B. Regarding cytoplasmic features, mixed and eosinophilic types were significantly observed in category 3, followed by category 2 ($p < 0.001$; Fig. 4B). The representative immunophenotype is shown in Fig. 4C. With respect to the tumor microenvironment, the inflamed and excluded immunophenotypes were significantly observed in category 3, followed by category 2 ($p < 0.001$; Fig. 4C).

The association of vascularity-based architectural classification with pathological factors of TCGA-KIRC cohort showed similar results of the principal cohort (Supplementary Fig. 6).

Regarding the gene signatures related to the response of VEGFR-TKIs and immunotherapy[26], the angiogenesis gene signature score was significantly enriched in category 1 compared to categories 2 and 3 ($p < 0.001$), whereas the signature scores of effector T-cell genes, immune checkpoint genes, and myeloid genes were significantly enriched in category 3 compared to categories 1 and 2 (all, $p < 0.001$) (Fig. 4D). We also confirmed the expression of hypoxia (*EPAS1*, known as *HIF2α*[28])- and angiogenesis (*CDH5*[23], *RGS5*[24], and *PDGFD*[29])-related genes were significantly enriched in category 1 than category 3 in the principal cohort (Supplementary Fig. 7).

Prognostic significance of vascularity-based architectural category

The Kaplan–Meier survival analysis showed a 5-year RFS rate of 77.0% (hazard ratio [HR] 5.62; 95% confidence interval [CI], 2.87–11.02; $p < 0.001$) for category 2 and 42.0% (HR 23.59; 95% CI, 11.11–50.08; $p < 0.001$) for category 3 versus 96.5% for category 1 (Fig. 5A). The RFS curves for each architectural pattern are shown in Supplementary Fig. 8. The survival curve of the TCGA-KIRC cohort was also stratified by patient's outcome (Supplementary Fig. 9). For the comparison of prognostic significance between vascularity-based architectural classification and the previously reported architectural grading system[6], we validated the proportion of each architectural pattern (Supplementary Table 2) and prognostic prediction according to the methods previously described[6]. Detailed information regarding architectural patterns of 3–tier and 4–tier architectural grades[6] and comparison of the grade corresponding to the patterns are shown in Supplementary Table 3. Although there was not a significant difference between grade 2 and grade 3 by a 4–tier architectural grade in our cohort, we confirmed the stratified RFS rates by a 3–tier architectural grade which was reported as a stronger prognostic predictor than a 4–tier grade[6] (Supplementary Fig. 10).

The association of clinicopathologic factors with recurrence after nephrectomy is shown in Table 2. In the univariate analysis, WHO/ISUP grade, necrosis, TNM stage, 3–tier architectural grade, and vascularity-based architectural classification was significantly associated with recurrence (all, $p < 0.001$). Vascularity-based architectural classification showed the best accuracy in predicting RFS (c-index = 0.786). On multivariate analysis, we established three models: Model 1, gathering three pathological factors (WHO/ISUP grade, necrosis, and TNM stage); Model 2, three pathological factors plus 3–tier architectural grade;[6] and Model 3, three pathological factors plus vascularity-based architectural classification. The vascularity-based architectural classification

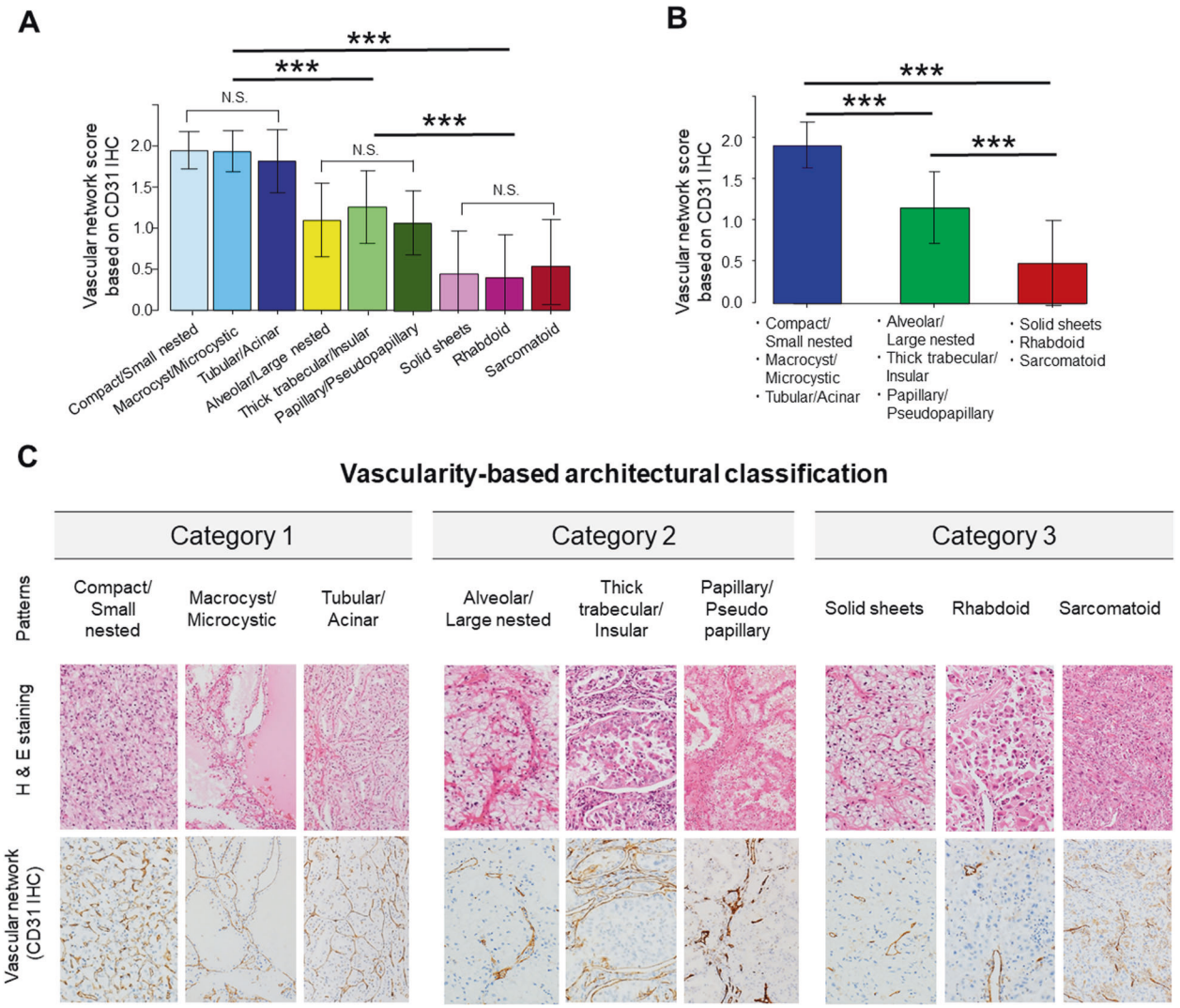

Fig. 3 Establishment of a vascularity-based architectural classification. A Association of nine architectural patterns with vascular network scores based on CD31 immunohistochemistry (IHC). **B** Architectural patterns were grouped into three categories by vascular network scores. **A**, **B** One-way analysis of variance with Tukey test or Kruskal–Wallis test was used for statistical analysis. ***$p < 0.001$. **C** Association of vascularity-based architectural classification with architectural patterns highlighted to vasculature by CD31 immunohistochemistry (IHC).

(HR 4.019; $p < 0.001$ and HR 3.259; $p = 0.049$) was identified as an independent prognostic factor for RFS as well as necrosis (HR 2.511; $p = 0.007$), and TNM stage (HR 5.479; $p < 0.001$). Model 3 (c-index = 0.871) showed the highest accuracy in predicting RFS versus Model 1 (c-index = 0.842) and Model 2 (c-index = 0.845).

Comparison of prognostic accuracy between our model and conventional risk models

Finally, we compared the predictive accuracy of RFS between our models and conventional risk models based on UISS, Leibovich score, and SSIGN score. Regarding the predictive ability of 5–year RFS, our model showed the highest accuracy than conventional risk models (c-index = 0.871 vs. 0.755–0.843; Fig. 5B).

DISCUSSION

In this study, we successfully established a vascularity-based architectural classification of ccRCC, which can be more easily evaluated with good interobserver reproducibility than the architectural grading system previously described and that can predict accurate recurrence after surgery. Additionally, the predictive accuracy of our model including WHO/ISUP grade, necrosis, and TNM stage was greater than conventional risk models such as UISS[19], Leibovich scores[2], and SSIGN scores[20]. Gene expression analysis related to the angiogenesis and immune biology gene signatures showed that vascularity-based architectural category 1 was significantly associated with angiogenesis gene signatures as compared to categories 2 and 3, whereas category 3 had significantly increased immune gene signatures than categories 1 and 2.

ccRCC is recognized as one of the most diverse tumors histologically, showing widespread intratumoral heterogeneity[3,7,32]. Cai and Christie et al.[7] revealed an average of three patterns per tumor, and 229 (41.7%) tumors showed prominent intratumoral heterogeneity with more than three patterns among nine distinct architectural patterns–(i) compact small nests, (ii) large nests, (iii) thick trabecular/insular, (iv) solid sheet, (v) microcystic, (vi) tubular/acinar, (vii) bleeding follicles, (viii) alveolar, and (ix) papillary/pseudopapillary. They found that the presence of a subset of architectural patterns such as alveolar, papillary, insular, and/or solid sheet components, regardless of the amount or presence of other patterns, was related to high nucleolar grade, high TNM stage, and frequently developed metastases. Considering their results, our methodology in which we captured the architectural patterns in the

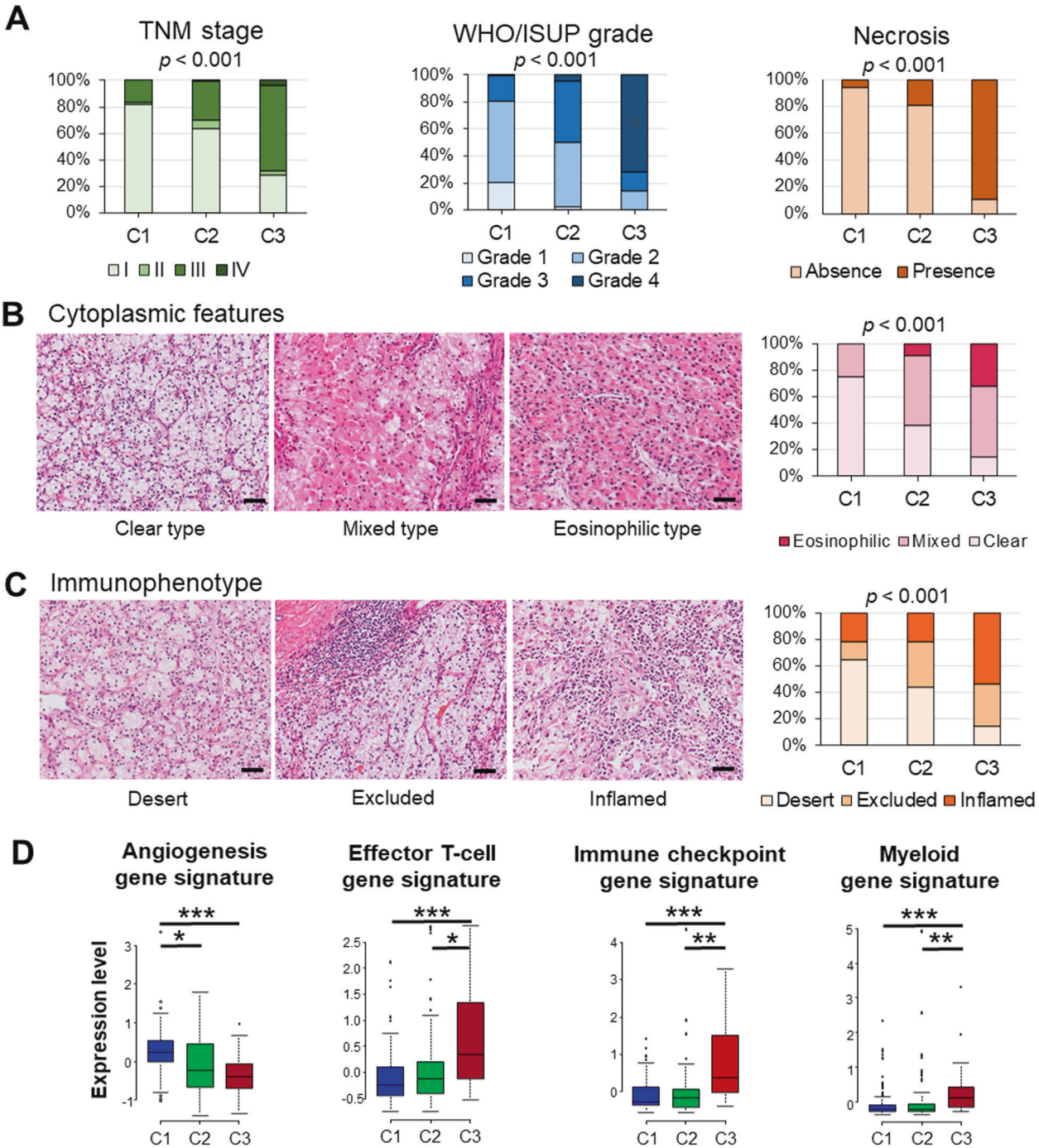

Fig. 4 Association of vascularity-based architectural classification with pathological factors in the principal cohort ($n = 436$) and gene expression signatures in the TCGA-KIRC cohort ($n = 162$). **A** Percentage of cases of each vascularity-based architectural classification and pathological prognostic factors. **B** Representative images of cytoplasmic features and percentage of cases of each vascularity-based architectural classification. Bar = 50 μm. **C** Representative images of immunophenotype and percentage of cases of each vascularity-based architectural classification. Bar = 50 μm. **D** Comparison of gene expression signature scores (mean Z-score) among vascularity-based architectural classification. WHO World Health Organization, ISUP International Society of Urological Pathology. Kruskal–Wallis test was used for statistical analysis (*$p < 0.05$, **$p < 0.01$, ***$p < 0.001$ assessed by Mann–Whitney test).

highest WHO/ISUP grade area shows correlation with prognosis and provides objective criteria for clinical application.

Although the association of architectural patterns and vascular networks has been previously shown[7], we established the vascularity-based architectural classification which statistically correlated with these relationships. For ensuring the objectivity of tumor vascularity, we defined a vascular network score based on the configuration of the vascularity using CD31 immunohistochemistry as previously described[7–9,18]. In various studies, microvessel density which is defined as the number of small vessels per tumor area, or microvessel area which is defined as the total lumen area of small vessels has been calculated by a digital analyzer to quantify the extent of tumor vascularization[8,18,22,33,34]. In this study, we demonstrated the correlation between vascular network score and microvessel area or angiogenesis-related gene expression as well as the prognostic

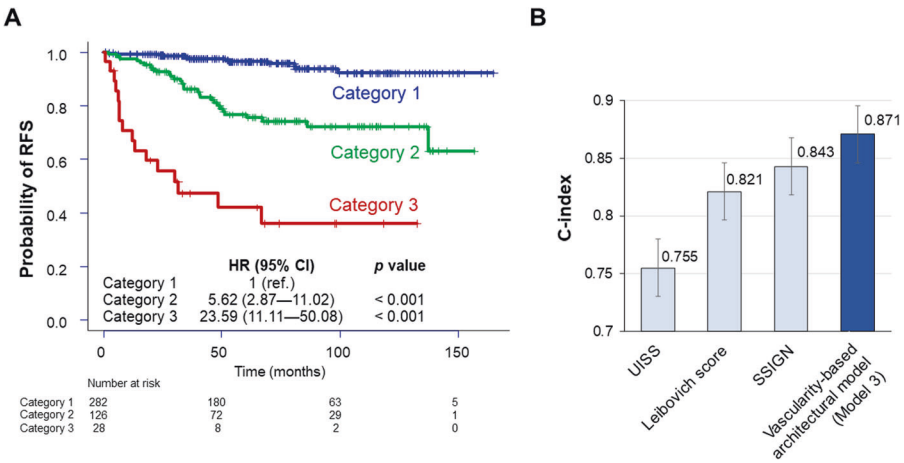

Fig. 5 Prognostic significance of vascularity-based architectural classification and comparison of accuracy between our models and conventional risk models. A Kaplan–Meier curve of recurrence-free survival (RFS). HR hazard ratio, CI confidence interval. **B** Concordance indices of University of California Los Angeles Integrated Staging System (UISS), Leibovich score, tumor stage, size, grade, and necrosis (SSIGN) score, and our vascularity-based architectural model.

ability of vascular network score. Therefore, we believe our methodology focusing only on the configuration of vascular networks has the advantage of simplicity and validity.

Nevertheless, we need not evaluate the vascular network score using CD31 immunohistochemistry in routine practice because the correlation between architectural patterns and vascular network score was confirmed in the present study. Interestingly, comparing the prognostic ability between vascularity-based architectural classification assessed by H&E staining and vascular network score by CD31 immunohistochemistry, vascularity-based architectural classification (c-index = 0.786) showed higher accuracy in predicting RFS than vascular network score (c-index = 0.72) (data not shown), which means a vascularity-based architectural classification is a more reliable prognostic prediction biomarker than vascular network score.

Our novel morphology-based classification based on the vascular network, which also reflects the previously described architectural grade[6] could stratify RFS rate for localized ccRCC. Cases with category 1 composed of compact/small nested, macrocyst/microcystic, and tubular/acinar patterns showed good prognosis and were compatible with previous results[6,7]. Although the patterns of vascularity-based architectural categories 2 and 3 were aggressive and similar to previously described results[7], the vascularity of a solid sheets pattern (vascular network score 0) was different from the vascularity of alveolar/large nested, thick trabecular/insular, or papillary/pseudopapillary patterns (vascular network score 1). The solid sheets pattern as well as sarcomatoid and rhabdoid features are considered as part of the final dedifferentiation pathway. Nevertheless, a small number of cases with vascularity-based architectural category 3 were detected in this study, and larger studies including ccRCC with solid sheets and rhabdoid/sarcomatoid patterns are needed to validate the clinical influence of our novel category.

We corroborated the underlying mechanism of category 3 tumors by gene expression analysis, which showed significantly down-regulated hypoxia- or angiogenesis-related genes. We also found that necrosis (displaying well-demarcated foci of necrotic granular cytoplasmic and nuclear debris with obliteration of the underlying architecture)[4] was also significantly associated with category 3. Because tumor necrosis results in a tumor outgrowing its own blood supply[35], the solid sheets pattern reflecting epithelial overgrowth without a vascular network may promote the development of necrosis.

Histologic grading of RCC has been recognized as a key prognostic factor since the time of Fuhrman's study for RCC grading[36]. Because methodological problems relating to the application, reproducibility, and validity of Fuhrman's grading system existed[37], the WHO/ISUP grade focusing on nucleolar prominence has been recommended for use[38]. Incorporating necrosis into the WHO/ISUP grading system for ccRCC demonstrated a greater predictive ability than the WHO/ISUP grade alone[39]. Indeed, these grading systems could stratify the prognosis of ccRCC patients both effectively and reproducibly as shown in various studies[40]. Nevertheless, while nucleolar grading shows good clinical utility, there is little knowledge on how it correlates with the underlying biologic potential of the tumor.

Recently, Verine et al. proposed a novel grading system for ccRCC based on 19 architectural patterns, which showed an independent prognostic value for both disease-free survival and cancer-specific survival (CSS), that outperformed all other morphologic grading systems[6]. Although we validated that their 3-tier grade system could stratify RFS rate of localized ccRCC, their architectural patterns are complex and less optimal to use because they include various histological features such as nuclear or cytological features, inflammatory reaction, and lymphatic invasion (shown in Supplementary Fig. 10), in addition to the architectural growth patterns. A recent report by Nilsson et al. firstly demonstrated a comparison of clear cell area and eosinophilic area in ccRCC by RNA-sequencing[8]. They revealed that the clear cell area displayed dense microvasculature, whereas eosinophilic areas were significantly less vascularized, highly proliferative, and with higher immune cell proliferation. In the agreement with the previous report[8], we first histologically show that the vascularity-based architectural classification is highly correlated with both clear or eosinophilic cytoplasmic features and immunophenotypes such as desert, excluded, and inflamed, defined based on the location of inflammatory cells[41].

A current clinical challenge for urologists is to identify patients who could derive a preferential benefit from therapeutic options[10,26]. Kapur et al. demonstrated the three conceptual 'axes', specifically, architectural patterns, cytological features and histopathological features of tumor microenvironment that could be used to more capably manage therapeutic approaches[7,42]. On the other hand, Nilsson et al. reported that the different gene expression of angiogenesis- and immune-associated genes between clear cell type and eosinophilic cell type of ccRCC would facilitate a potential therapeutic strategy of VEGFR-TKIs or immune therapies[8]. Subsequently, our prior study has recently shown that histological phenotypes such as clear, mixed or eosinophilic types, which have different underlying mechanisms, correlated with

Table 2. Cox regression analysis of prognostic factors for predicting recurrence-free survival in ccRCCs of the principal cohort.

Variables	Univariate		Model 1			Model 2			Model 3		
	p-value	*c*-index	HR	95% CI	*p*-value	HR	95% CI	*p*-value	HR	95% CI	*p*-value
Age, years (continuous)	0.210	0.552									
Gender (female vs. male)	0.900	0.493									
WHO/ISUP grade		0.718									
Grade 1/2	—		1 (ref.)			1 (ref.)			1 (ref.)		
Grade 3	<0.001		1.413	0.73–2.74	0.307	1.45	0.74–2.84	0.279	1.279	0.68–2.41	0.446
Grade 4	<0.001		4.309	1.82–10.18	<0.001	2.649	0.70–10.01	0.151	2.979	1.00–8.89	0.050
Necrosis (absent vs. present)	<0.001	0.737	2.791	1.41–5.53	0.003	2.681	1.32–5.45	0.006	2.511	1.28–4.93	0.007
TNM stage (<III vs. ≥III)	<0.001	0.759	5.941	3.22–10.95	<0.001	5.895	3.17–10.97	<0.001	5.479	2.97–10.12	<0.001
3-tier architectural grade*		0.643									
Grade 1	—					1 (ref.)					
Grade 2	0.02					0.905	0.36–2.25	0.830			
Grade 3	<0.001					3.187	0.86–11.81	0.083			
Vascularity-based architectural classification		0.786									
Category 1	—								1 (ref.)		
Category 2	<0.001								4.019	2.03–7.94	<0.001
Category 3	<0.001								3.259	1.01–10.57	0.049
c-index (multivariate model)	—		0.842			0.845			0.871		

ccRCC clear cell renal cell carcinoma, HR hazard ratio, CI confidence interval, WHO World Health Organization, ISUP International Society of Urological Pathology, * [6].

survival outcome and response to angiogenesis and checkpoint blockade in ccRCC patients[18]. In the present study, we validated the association of vascularity-based architectural classification with gene expression signatures, which could discriminate potential relevance for application of angiogenesis and immunotherapy[26], using the TCGA-KIRC cohort. The vascularity-based architectural classification corresponded to not only angiogenesis but also immune gene signatures. Considering all these findings, our vascularity-based architectural classification would be expected to comprehensively provide prognostic information and function as a surrogate for treatment selection of ccRCC.

Our study has several limitations. First, this is a retrospective, single-center study. Although we successfully validated our model using the TCGA cohort, validation analysis across multiple institutions is needed. Second, CD31 immunohistochemistry was evaluated in tissue microarray specimens including only the highest-grade area. Third, different gene expression panels were used between principal and TCGA-KIRC cohorts. Fourth, the candidate for the principal cohort was localized ccRCC patients, of which the only endpoint was RFS, not CSS or overall survival (OS). On the other hand, the candidate for the TCGA-KIRC cohort included metastatic ccRCC patients, of which the only available endpoint was OS. Despite these limitations, we showed that our vascularity-based architectural classification could capture the underlying genomics of ccRCC including cancer immunity.

In conclusion, the vascularity-based architectural classification correlated with clear or eosinophilic cytoplasmic features and immunophenotype as well as pathological prognostic factors such as TNM stage, WHO/ISUP grade, and necrosis, and showed better prognostic prediction than the grading system previously described. Our proposed vascularity-based architectural classification also correlated with gene expression signatures of both angiogenesis and tumor immunity and hence in addition to the prognostic value for risk stratification, and also may have predictive implications as it could be applied to guide future clinical planning regarding adjuvant therapy for those at risk for recurrence.

DATA AVAILIABILITY

The data are available upon reasonable request by contacting the corresponding author.

REFERENCES

1. Shuch, B. et al. Understanding pathologic variants of renal cell carcinoma: distilling therapeutic opportunities from biologic complexity. *Eur. Urol.* **67**, 85–97 (2015).
2. Leibovich, B. C. et al. Prediction of progression after radical nephrectomy for patients with clear cell renal cell carcinoma: a stratification tool for prospective clinical trials. *Cancer* **97**, 1663–1671 (2003).
3. Moch H., Humphrey P. A., Ulbright T. M., Reuter V. E. *WHO Classification of Tumours of the Urinary System and Male Genital Organs* 4th edn (IARC, 2016).
4. Delahunt, B. et al. Data set for the reporting of carcinoma of renal tubular origin: recommendations from the International Collaboration on Cancer Reporting (ICCR). *Histopathology* **74**, 377–390 (2019).
5. Tretiakova, M. S. Renal cell tumors: molecular findings reshaping clinico-pathological practice. *Arch. Med. Res.* **51**, 799–816 (2020).
6. Verine, J. et al. Architectural patterns are a relevant morphologic grading system for clear cell renal cell carcinoma prognosis assessment. *Am. J. Surg. Pathol.* **42**, 423–441 (2018).
7. Cai, Q. et al. Ontological analyses reveal clinically-significant clear cell renal cell carcinoma subtypes with convergent evolutionary trajectories into an aggressive type. *EBioMedicine* **51**, 102526 (2020).

8. Nilsson, H. et al. Features of increased malignancy in eosinophilic clear cell renal cell carcinoma. *J. Pathol.* **252**, 384–397 (2020).
9. Ing, N. et al. A novel machine learning approach reveals latent vascular phenotypes predictive of renal cancer outcome. *Sci. Rep.* **7**, 13190 (2017).
10. Smith, S. C. & Amin, M. B. Assessment of intratumoral histologic heterogeneity in clear cell renal cell carcinoma: opportunities to inform molecular studies and therapeutic approach? Kidney. *Cancer J.* **18**, 85–86 (2020).
11. Broad GDAC FIREHOSE-Broad Institute. Available online: http://gdac.broadinstitute.org/ (accessed on August 2021).
12. Ricketts, C. J. et al. The Cancer Genome Atlas comprehensive molecular characterization of renal cell carcinoma. *Cell Rep.* **23**, 313–326.e5 (2018).
13. Digital Slide Archive (DSA). Available online: https://cancer.digitalslidearchive.org/ (accessed on August 2021).
14. Brierley J. D., Gospodarowics M. K., Wittekind C. Union for International Cancer Control. *TNM Classification of Malignant Tumours* 8th edn (Wiley, 2017).
15. Yoshida, T. et al. Clinical impact of segmental renal vein invasion on recurrence in patients with clinical T1 renal cell carcinoma undergoing partial nephrectomy. *Int. J. Clin. Oncol.* **25**, 464–471 (2020).
16. Ohsugi, H. et al. The SSPN Score, a novel scoring system incorporating PBRM1 expression, predicts postoperative recurrence for patients with non-metastatic clear cell renal cell carcinoma. *Ann. Surg. Oncol.* **28**, 2359–2366 (2021).
17. Yoshida, T. et al. Integration of NRP1, RGS5, and FOXM1 expression, and tumour necrosis, as a postoperative prognostic classifier based on molecular subtypes of clear cell renal cell carcinoma. *J. Pathol. Clin. Res.* **7**, 590–603 (2021).
18. Yoshida, T. et al. Eosinophilic features in clear cell renal cell carcinoma correlate with outcomes of immune checkpoint and angiogenesis blockade. *J. Immunother. Cancer* **9**, e002922 (2021).
19. Zisman, A. et al. Improved prognostication of renal cell carcinoma using an integrated staging system. *J. Clin. Oncol.* **19**, 1649–1657 (2001).
20. Frank, I. et al. An outcome prediction model for patients with clear cell renal cell carcinoma treated with radical nephrectomy based on tumor stage, size, grade, and necrosis: the SSIGN score. *J. Urol.* **168**, 2395–2400 (2002).
21. Hedge, P. S., Karanikas, V. & Evers, S. The where, then when, and the how of immune monitoring for cancer immunotherapies in the era of checkpoint inhibition. *Clin. Cancer Res.* **22**, 1865–1874 (2016).
22. Sullivan, C. A. et al. Microvessel area using automated image analysis is reproducible and is associated with prognosis in breast cancer. *Hum. Pathol.* **40**, 156–165 (2009).
23. Sauteur, L. et al. Cdh5/VE-cadherin promotes endothelial cell interface elongation via cortical actin polymerization during angiogenic sprouting. *Cell Rep.* **9**, 504–513 (2014).
24. Furuya, M. et al. Expression of regulator of G protein signalling protein 5 (RGS5) in the tumour vasculature of human renal cell carcinoma. *J. Pathol.* **203**, 551–558 (2004).
25. Ohashi, R. et al. Loss of CDKN1A mRNA and protein expression are independent predictors of poor outcome in chromophobe renal cell carcinoma patients. *Cancers* **12**, 465 (2020).
26. McDermott, D. F. et al. Clinical activity and molecular correlates of response to atezolizumab alone or in combination with bevacizumab versus sunitinib in renal cell carcinoma. *Nat. Med.* **24**, 749–757 (2018).
27. Bolen, C. R. et al. Mutation load and an effector T-cell gene signature may distinguish immunologically distinct and clinically relevant lymphoma subsets. *Blood Adv.* **22**, 1884–1890 (2017).
28. Pietras, A., Johnsson, A. S. & Påhlman, S. The HIF-2α-driven pseudo-hypoxic phenotype in tumor aggressiveness, differentiation, and vascularization. *Curr. Top. Microbiol. Immunol.* **345**, 1–20 (2010).
29. Xu, L., Tong, R., Cochran, D. M. & Jain, R. K. Blocking platelet-derived growth factor-D/platelet-derived growth factor receptor beta signaling inhibits human renal cell carcinoma progression in an orthotopic mouse model. *Cancer Res.* **65**, 5711–5719 (2005).
30. Brooks, S. A. et al. ClearCode34: a prognostic risk predictor for localized clear cell renal cell carcinoma. *Eur. Urol.* **66**, 77–84 (2014).
31. Kanda, Y. Investigation of the freely available easy-to-use software'EZR' for medical statistics. *Bone Marrow Transpl.* **48**, 452–458 (2013).
32. Gulati, S. et al. Systematic evaluation of the prognostic impact and intratumour heterogeneity of clear cell renal cell carcinoma biomarkers. *Eur. Urol.* **66**, 936–948 (2014).
33. Sabo, E. et al. Microscopic analysis and significance of vascular architectural complexity in renal cell carcinoma. *Clin. Cancer Res.* **7**, 533–537 (2001).
34. Sato, M. et al. Microvessel area of immature vessels is a prognostic factor in renal cell carcinoma. *Int. J. Urol.* **21**, 130–134 (2014).
35. Sengupta, S. et al. Histologic coagulative tumor necrosis as a prognostic indicator of renal cell carcinoma aggressiveness. *Cancer* **104**, 511–520 (2005).
36. Fuhrman, S. A., Lasky, L. C. & Limas, C. Prognostic significance of morphologic parameters in renal cell carcinoma. *Am. J. Surg. Pathol.* **6**, 655–663 (1982).
37. Al-Aynati, M. et al. Interobserver and intraobserver variability using the Fuhrman grading system for renal cell carcinoma. *Arch Pathol. Lab. Med.* **127**, 593–596 (2003).
38. Delahunt, B. et al. Grading of clear cell renal cell carcinoma should be based on nucleolar prominence. *Am. J. Surg. Pathol.* **35**, 1134–1139 (2011).
39. Delahunt, B. et al. A novel grading system for clear cell renal cell carcinoma incorporating tumor necrosis. *Am. J. Surg. Pathol.* **37**, 311–322 (2013).
40. Delahunt, B., Eble, J. N., Egevad, L. & Samaratunga, H. Grading of renal cell carcinoma. *Histopathology* **74**, 4–17 (2019).
41. Brück O., et al. Spatial immunoprofiling of the intratumoral and peritumoral tissue of renal cell carcinoma patients. *Mod. Pathol.* https://doi.org/10.1038/s41379-021-00864-0 (2021).
42. Kapur, P., Christie, A., Rajaram, S. & Brugarolas, J. What morphology can teach us about renal cell carcinoma clonal evolution. *Kidney Cancer J.* **18**, 68–76 (2020).

ACKNOWLEDGEMENTS

We are grateful to Ms. Linjun Zha for her assistance in immunohistochemistry and Mr. Ryousuke Yamaka for his technical assistance in the construction of tissue microarray, tissue sampling, and NanoString assay. This work was supported by the research grant from Kansai Medical University (KMU) research consortium. This study has supported by the Japan Society for the Promotion of Science KAKENHI fund (Grants No. 19K16875 to CO, and Grants No. 20K16457 to HO).

AUTHOR CONTRIBUTIONS

Conception and design: C.O., T.Y. Acquisition, analysis, or interpretation of data: CO, T. Y., N.A., J.I., K.S., Y.N., Y.Y., R.O., H.O. Study supervision: M.A., H.K., K.H., K.T. Manuscript writing: C.O. Final approval of manuscript: All authors.

ETHICS APPROVAL

This study was performed in accordance with the Declaration of Helsinki. The ethics committee of Kansai Medical University approved this study (No. 2018109 and No. 2020222).

COMPETING INTERESTS

CO received research funding from Chugai Pharmaceutical Co. Ltd. outside the submitted work. The remaining authors have no conflict of interest.

ADDITIONAL INFORMATION

Supplementary information The online version contains supplementary material available at https://doi.org/10.1038/s41379-021-00982-9.

Correspondence and requests for materials should be addressed to Chisato Ohe.

Reprints and permission information is available at http://www.nature.com/reprints

Publisher's note Springer Nature remains neutral with regard to jurisdictional claims in published maps and institutional affiliations.